Atmos. Chem. Phys. Discuss., https://doi.org/10.5194/acp-2018-753
Manuscript under review for journal Atmos. Chem. Phys.
Discussion started: 30 July 2018

Atmospheric Chemistry and Physics Discussions

Aerosol hygroscopic growth, contributing factors and impact on haze events in a severely polluted region in northern China

Jun Chen[1], Zhanqing Li[1,2,*], Min Lv[3], Yuying Wang[1], Wei Wang[1], Yingjie Zhang[4], Haofei Wang[5,6], Xing Yan[1], Yele Sun[4], Maureen Cribb[2]

[1]State Key Laboratory of Earth Surface Processes and Resource Ecology, College of Global Change and Earth System Science, Beijing Normal University, Beijing 100875, China
[2]Department of Atmospheric and Oceanic Sciences and ESSIC, University of Maryland, College Park, Maryland, USA
[3]School of Geographic Science, Nantong University, Nantong 226000, China
[4]State Key Laboratory of Atmospheric Boundary Layer Physics and Atmospheric Chemistry, Institute of Atmospheric Physics, Chinese Academy of Sciences, Beijing 100029, China
[5]College of Resource Environment and Tourism, Capital Normal University, Beijing, 100048, China
[6]State Environment Protection Key Laboratory of Satellite Remote Sensing, Institute of Remote Sensing and Digital Earth, Chinese Academy of Sciences, Beijing, 100101, China

Correspondence to: Zhanqing Li (zli@atmos.umd.edu)

To be submitted to the ACP Special Section on Air Pollution in China

July 17, 2018

Atmos. Chem. Phys. Discuss., https://doi.org/10.5194/acp-2018-753
Manuscript under review for journal Atmos. Chem. Phys.
Discussion started: 30 July 2018

Atmospheric Chemistry and Physics Discussions

Abstract:

The hygroscopic growth of aerosol particles is a key factor of air pollution because it can significantly reduce visibility. In order to better understand the impact of the hygroscopic growth effect on haze events and contributing factors, we made use of rich measurements during an intensive field campaign conducted in Xingtai, Hebei province of China that has suffered from the most serious pollution in the Northern China Plain. Key measurements are from Raman lidar and ground-based instruments such as a GrayWolf 6-channel handheld particle/mass meter for atmospheric particulate matter that have diameters less than 1 μm and 2.5 μm (PM_1 and $PM_{2.5}$, respectively), aerosol chemical speciation monitor (ACSM), and a hygroscopic tandem differential mobility analyzer (H-TDMA). The evolution of PM_1 and $PM_{2.5}$ agreed well with that of the water vapor content due to the aerosol hygroscopic growth effect. Two cases were selected to further analyze the effects of aerosol particle hygroscopic growth on haze events. The lidar-estimated aerosol hygroscopic enhancement factor during a pollution event (Case II) was greater than that during a relatively clean period (Case I) with similar relative humidity (RH): 80–91%. The hygroscopic growth was fitted by the Kasten model whose parameter *b* differ considerably: 0.9346 vs. 0.1000 for cases II and I respectively. The aerosol acidity value of Case II (1.50) was greater than that of Case I (1.35) due to different amounts of inorganics such as NH_4NO_3, NH_4HSO_4, and $(NH_4)_2SO_4$, consistent with the difference in the aerosol hygroscopicity parameter κ calculated from the chemical species of PM_1 obtained by the ACSM. Data from the H-TDMA showed that all of the aerosol particle size hygroscopic growth factors in each particle size category

Atmos. Chem. Phys. Discuss., https://doi.org/10.5194/acp-2018-753
Manuscript under review for journal Atmos. Chem. Phys.
Discussion started: 30 July 2018

Atmospheric Chemistry and Physics Discussions

(40, 80, 110, 150, and 200 nm) at different RH (80–91%) during Case II were higher than those during Case I. Under the same water vapor conditions, aerosol hygroscopic growth was one of the major factors contributing to heavy haze pollution. Concerning aerosol chemical composition, nitrate was the primary component contributing to aerosol hygroscopicity over Xingtai.

Key words: Raman lidar; aerosol hygroscopic growth; water content; haze; remote sensing

Atmos. Chem. Phys. Discuss., https://doi.org/10.5194/acp-2018-753
Manuscript under review for journal Atmos. Chem. Phys.
Discussion started: 30 July 2018

Atmospheric Chemistry and Physics Discussions

1. Introduction

Atmospheric aerosol particles are one of the most important components of the atmosphere that play a key role in Earth's climate system, mainly because aerosol particles can directly and strongly scatter and absorb visible light (Mie, 1908). Moreover, atmospheric aerosol particles can act as cloud condensation nuclei and ice nuclei, a process that might change cloud optical and microphysical properties (Twomey, 1977). Atmospheric aerosol particles through hygroscopic growth can influence air quality and visibility (Haywood et al., 2008; Y.-F., Wang et al., 2012; Y.-Y. Wang et al., 2017). Hygroscopic growth is a process whereby the aerosol scattering capacity increases significantly at high relative humidity (RH) levels, leading to enlarged aerosol particles (Covert et al., 1972; Hänel, 1976; Jeong et al., 2007). A recent study on the 2012–2013 winter haze events in Beijing (Tie et al., 2017) showed that atmospheric water vapor plays a critical role in the formation of severe haze events in China and that aerosol hygroscopic growth is one of the crucial factors in enhancing heavy haze events.

The hygroscopic growth factor (GF) measures the change in particle diameter due to water uptake that can be measured by a humidified tandem differential mobility analyzer (H-TDMA) (e.g., Liu et al., 1978; Swietlicki et al., 2008; Y.-Y. Wang et al., 2017). The aerosol hygroscopic optical enhancement factor [$f(RH)$] has also also been employed, defined as the ratio between aerosol optical properties (e.g., aerosol extinction coefficient, total scattering and backscattering coefficients) under wet atmospheric conditions and the corresponding reference value under dry conditions (Kotchenruther et al., 1999). It can be measured by a humidified tandem nephelometer (e.g., Covert et al., 1972; Feingold and Morley, 2003; Titos et al., 2018).

Atmos. Chem. Phys. Discuss., https://doi.org/10.5194/acp-2018-753
Manuscript under review for journal Atmos. Chem. Phys.
Discussion started: 30 July 2018

MacKinnon (1969) found that the lidar backscattering signal is affected by the environmental RH level. Subsequent studies demonstrated the use of lidar for observing the aerosol hygroscopic growth phenomenon (Tardif et al., 2003; Pahlow et al., 2006; Veselovskii et al., 2009; Di Girolamo et al., 2012; Fernández et al., 2015; Granados-Muñoz et al., 2015; Bedoya-Velásquez et al., 2018; Lv et al., 2017).

Raman lidar is particularly valuable for measuring atmospheric water vapor by using the vibrational Raman scattering signal from water vapor molecules (H_2O) and nitrogen molecules (N_2) (Whiteman, 2003; Barnes et al., 2008). Many ground-based Raman lidar systems have been operated in the world for measuring both atmospheric water vapor and aerosol profiles (Leblanc et al., 2012; Froidevaux et al., 2013; Wang et al., 2015; Bedoya-Velásquez et al., 2018). The Lidar technology allows for measurements under unmodified ambient atmospheric conditions instead of drying and then humidifying air samples that may alter aerosol physical and chemical properties, a major limitation for in situ observation techniques such as the H-TDMA and nephelometer (Bedoya-Velásquez et al., 2018). Raman lidar systems also provide measurements at higher spatial and temporal resolutions which are useful for examining the effects of aerosol hygroscopic growth on pollution events (e.g., Y.-F. Wang et al., 2012, 2017; Su et al., 2017). Despite the numerous studies, these factors are still poorly known, especially their influential factors in terms of aerosol chemical composition.

Xingtai is a city with high density of heavy industries that has been frequently ranked as one of the most polluted cities in China. We have thus attempted to gain deeper insights into the physical, chemical, optical and hygroscopic properties of aerosol particles in order to understand the causes and evolution of pollution in the region. A specific goal of this study is

Atmos. Chem. Phys. Discuss., https://doi.org/10.5194/acp-2018-753
Manuscript under review for journal Atmos. Chem. Phys.
Discussion started: 30 July 2018

to study the hygroscopic growth factor and its controlling factor for atmospheric particulate matter that have diameters less than 1 μm and 2.5 μm (PM_1 and $PM_{2.5}$, respectively) based on Raman lidar measurements made at Xingtai in late May 2016 together with other suites of instruments measuring a variety of aerosol properties. Two representative cases are also selected to single out the influences of aerosol chemical compositions.

The following section describes the field experiment, instruments and data used. Section 3 presents the methodology and Section 4 describes the results. A brief summary of this study is given in Section 5.

2. Field campaign and instruments

In order to analyze the relationship between the atmospheric water vapor content and the PM_1 and $PM_{2.5}$ mass concentrations, and to explore the atmospheric aerosol particle hygroscopic growth effect on haze events, a Raman lidar was used. The lidar is an automated system that retrieves atmospheric water vapor mixing ratios (W) and aerosol optical property profiles throughout the day. The lidar system used in this study emits three laser beams simultaneously at 355, 532, and 1064 nm with a time resolution of 15 min and a range resolution of 7.5 m. The optical receiving unit includes an ultraviolet telescope and a visible infrared telescope. The ultraviolet telescope received atmospheric Mie scattering signals and vibrational Raman scattering signals from H_2O and N_2 molecules (at 355, 386, and 407 nm). The atmospheric Mie scattering signal at 532 nm and 1064 nm is received by the visible infrared telescope.

Atmos. Chem. Phys. Discuss., https://doi.org/10.5194/acp-2018-753
Manuscript under review for journal Atmos. Chem. Phys.
Discussion started: 30 July 2018

Collocated radiosondes were launched twice a day, i.e., at ~0715 and ~1915 Beijing Time (BJT), during the field campaign. The GTS1 detector collected profiles of atmospheric RH, temperature, and pressure at a resolution of 1%, 0.1ºC, and 0.1 hPa, respectively. The radiosonde ascension velocity was ~5–6 m s^{-1}.

A collocated Doppler lidar system (TWP3-M) was also in operation at Xingtai. This system provides time series of horizontal wind velocity, horizontal wind direction, and vertical wind speed at a time resolution of 5 min and a range resolution of 60 m below 1 km and 120 m above 1 km. The maximum and minimum detection distances of this system are 3–5 km and 0.1 km, respectively.

AGrayWolf 6-channel handheld particle/mass meter (PC-3016A) was used to monitor the mass concentrations of $PM_{2.5}$ and PM_1 (Yan et al., 2017). An aerosol chemical speciation monitor (ACSM) measures aerosol chemical composition (organics, sulfate, nitrate, ammonium, chloride) at a time resolution of five minutes. Detailed information about the operations of the ACSM and data analysis can be found elsewhere (e.g., Sun et al., 2016; Zhang et al., 2016, 2017). The aerosol GF at RH = ~85% was retrieved by an H-TDMA. The H-TDMA used in this study has also been described in more details in Y.-Y. Wang et al. (2017). All data are reported in Beijing local time in this study.

3. Methodology

3.1 Water vapor retrieval

Using the ratio of the Raman signals of H_2O (P_H) and N_2 (P_N), atmospheric water vapor content (*W*) can be calculated as follows (Melfi, 1972; Leblanc et al., 2012; Su et al., 2017):

Atmos. Chem. Phys. Discuss., https://doi.org/10.5194/acp-2018-753
Manuscript under review for journal Atmos. Chem. Phys.
Discussion started: 30 July 2018

Atmospheric Chemistry and Physics Discussions

$$W(z) = C_W \Delta q \frac{P_H(z)}{P_N(z)} \quad , \tag{1}$$

$$\Delta q = \frac{\exp[-\int_0^z (\alpha_N^m + \alpha_N^p) dz]}{\exp[-\int_0^z (\alpha_H^m + \alpha_H^p) dz]} \quad , \tag{2}$$

where C_W is the Raman lidar calibration constant which can be calculated using corresponding radiosonde data (Melfi, 1972; Sherlock et al., 1999). The parameters α_N^m and α_H^m are the molecular extinction coefficients at 386 nm and 407 nm, respectively. These can also be calculated using temperature and pressure profiles from radiosonde measurements (Bucholtz, 1995). The parameters α_N^p and α_H^p are the aerosol extinction coefficients (AECs) at 386 nm and 407 nm, respectively. Here, we use the Fernald method to retrieve AECs (Fernald, 1984). Note that during the daytime, the height of the retrieved *W* profile will be limited because the Raman signal is affected by radiation (Tobin et al., 2012).

We can also calculate the vertical distribution of RH based on the vertical profile of *W* retrieved from Raman lidar measurements and the temperature and pressure profiles provided by radiosonde data. The following equations are used to retrieve the RH profile:

$$RH(z) = \left[\frac{e(z)}{e_s(z)}\right] \times 100\%, \tag{3}$$

$$e(z) = \frac{W(z)p(z)}{0.622 + W(z)}, \tag{4}$$

$$e_s(z) = 6.1078 \exp\left[\frac{17.13[T(z) - 273.16]}{T(z) - 38}\right], \tag{5}$$

where $e(z)$ and $e_s(z)$ are the vertical profiles of water vapor pressure (in hPa) and saturation vapor pressure (in hPa) at a certain temperature, respectively, *W(z)* is the *W* profile obtained

Atmos. Chem. Phys. Discuss., https://doi.org/10.5194/acp-2018-753
Manuscript under review for journal Atmos. Chem. Phys.
Discussion started: 30 July 2018

from the Raman lidar, $p(z)$ is the pressure profile (in hPa), and $T(z)$ is the temperature profile (in Kelvin) provided by radiosonde data.

To assess the accuracy of the retrieval algorithm, Raman lidar- and radiosonde-derived W profiles at 0515 BJT on 24 May 2016 and their differences are shown in Fig. 1. The W profiles agree well with an absolute error between them of less than 0.5 g kg^{-1}. Figure 2 shows results of the vertical profiles of RH retrieved by the Raman lidar and the Radiosonde at 0515 BJT 24 May 2016. Absolute errors between Raman lidar- and radiosonde-derived RH profiles are generally less than 5%. Figures 1 and 2 suggest that the retrieval algorithm can produce reasonable results.

3.2 Selection of aerosol hygroscopic cases and their optical properties

How aerosol particle hygroscopic growth cases were chosen is described here. First, atmospheric mixing conditions were examined using radiosonde-based vertical potential temperature (θ) and W profiles. Cases with near-constant values of θ and W in the analyzed layer (variations less than 2°C and 2 g kg^{-1}, respectively) represent good atmospheric mixing conditions (Granados-Muñoz et al., 2015). Then aerosol backscattering coefficient profiles at 532 nm were calculated based on the Fernald method (Fernald, 1984). Cases were chosen with a simultaneous increase in atmospheric RH and aerosol backscattering coefficient. These steps are needed to ensure that the variations in aerosol properties are due to water uptake and not to changes in the aerosol load (Bedoya-Velásquez et al., 2018). Aerosol hygroscopic properties of the selected cases were investigated in terms of the enhancement factor for the backscattering coefficient which is defined as follows:

Atmos. Chem. Phys. Discuss., https://doi.org/10.5194/acp-2018-753
Manuscript under review for journal Atmos. Chem. Phys.
Discussion started: 30 July 2018

Atmospheric Chemistry and Physics Discussions

$$f_\beta(RH,\lambda)=\frac{\beta(RH,\lambda)}{\beta(RH_{ref},\lambda)}\ , \tag{6}$$

where $\beta(RH,\lambda)$ and $\beta(RH_{ref},\lambda)$ represent aerosol backscattering coefficients at a certain RH value and at a reference RH value, respectively, at wavelength λ. In this study, we selected $RH_{ref}=80\%$ which is the lowest RH in the layer to be analyzed.

Finally, a two-parameter fit equation was used to obtain the relationship between RH and $f_\beta(RH)$ (Kasten, 1969):

$$f_\beta(RH)=a(1-RH)^{-b}, \tag{7}$$

where a and b are the hygroscopic parameters that define the enhancement. The larger the value of b is, the more hygroscopic are the particles (Fernández et al., 2015). The Hänel model (Hänel et al., 1976) was also used to calculate $f_\beta(RH)$:

$$f_\beta(RH)=\left(\frac{1-RH}{1-RH_{ref}}\right)^{-\gamma}. \tag{8}$$

Larger γ values in this formulation denotes stronger hygroscopic growth. Whichever model had the best fit to the data was selected.

3.3 Calculation of aerosol particle acidity

The acidity of aerosol particles is a key parameter affecting aerosol hygroscopic growth (Sun et al., 2009; Lv et al., 2017). Acidic aerosols in the atmosphere tend to be more hygroscopic than their neutralized form (Zhang et al., 2007). High hygroscopicity of aerosol particles enhances their ability to scatter light. We examined acidity by comparing the measured NH_4^+ mass concentration and the amount needed to fully neutralize sulfate, nitrate, and chloride ions ($NH_{4\ predicted}^+$) (Sun et al., 2009; Zhang et al., 2015; Lv et al., 2017):

Atmos. Chem. Phys. Discuss., https://doi.org/10.5194/acp-2018-753
Manuscript under review for journal Atmos. Chem. Phys.
Discussion started: 30 July 2018

Atmospheric Chemistry and Physics Discussions

$$NH_{4\ predicted}^{+} = (2\times SO_4^{2-}/96 + NO_3^{-}/62 + Cl^{-}/35.5)\times 18, \quad (9)$$

where SO_4^{2-}, NO_3^{-} and Cl^{-} represent the mass concentrations (in μg m^{-3}) of the three species. The molecular weights of SO_4^{2-}, NO_3^{-}, Cl^{-} and NH_4^{+} are 96, 62, 35.5, and 18, respectively. Aerosol particles are considered "more acidic" if the measured NH_4^{+} mass concentration is significantly lower than that of the predicted NH_4^{+}. Aerosol particles are considered "bulk neutralized" if the two values are similar (Zhang et al., 2007; Sun et al., 2009; Zhang et al., 2015; Lv et al., 2017).

The acidity of aerosol particles can be measured by the parameter acid value (*AV*) (Zhang et al., 2007) defined as follows:

$$AV = (2\times SO_4^{2-}/96 + NO_3^{-}/62 + Cl^{-}/35.5)/(NH_4^{+}/18). \quad (10)$$

Aerosol particles are considered "bulk neutralized" if $AV = 1$ and "strong acidic" if $AV > 1.25$. When $AV = 1.25$, 50% of the total sulfate ions in the atmosphere consists of NH_4HSO_4 and the other 50% consist of $(NH_4)_2SO_4$.

3.4 Aerosol chemical ion-pairing scheme

Zieger et al. (2014) showed that the magnitude of $f(RH)$ is correlated with the inorganic mass fraction. However, the GFs differ with different inorganic salts. To examine the mass fractions of neutral inorganic salts, ACSM measurements were used to calculate mass concentrations and volume fractions (Gysel et al., 2007). This approach is based on an ion-pairing scheme introduced by Reilly and Wood (1969). Because the ACSM mainly measures the mass concentrations of SO_4^{2-}, NO_3^{-}, NH_4^{+}, Cl^{-} and organics, the chlorine ion was not considered because its concentration is extremely low. The aerosol chemical ion combination

Atmos. Chem. Phys. Discuss., https://doi.org/10.5194/acp-2018-753
Manuscript under review for journal Atmos. Chem. Phys.
Discussion started: 30 July 2018

scheme is given by the following equations:

$$\begin{aligned} n_{NH_4NO_3} &= n_{NO_3^-} \\ n_{NH_4HSO_4} &= \min(2n_{SO_4^{2-}} - n_{NH_4^+} + n_{NO_3^-}, n_{NH_4^+} - n_{NO_3^-}) \\ n_{(NH_4)_2SO_4} &= \max(n_{NH_4^+} - n_{NO_3^-} - n_{SO_4^{2-}}, 0) \\ n_{H_2SO_4} &= \max(0, n_{SO_4^{2-}} - n_{NH_4^+} + n_{NO_3^-}) \\ n_{HNO_3} &= 0 \end{aligned} \quad , \tag{11}$$

where n donates the number of the moles, "min" and "max" are minimum and maximum values (Gysel et al., 2007). The volume fractions of inorganic salts can be calculated based on the ion combination scheme and the parameters in Table 1. Furthermore, for a multicomponent particle, the Zdanovskii-Stocks-Robinson mixing rule (Zdanovskii, 1948; Stokes and Robinson, 1966) can be applied to calculate the hygroscopicity parameter κ:

$$\kappa = \sum_i \varepsilon_i \kappa_i \quad . \tag{12}$$

where κ_i is the hygroscopicity parameter of each individual component. The parameter ε_i is the volume fraction of each component.

4. Results and discussion

4.1 Observations of *W* and mass concentrations of PM_1 and $PM_{2.5}$

Figure 3a shows the time series of the lidar-derived *W* at Xingtai from 19–31 May 2016. The height of the retrieved *W* profile was limited because of the solar radiation during the daytime (Tobin et al., 2012). Overall, *W* was generally less than 6 g kg^{-1} with a strong daily variability during the analyzed period. The simultaneous temporal evolution of the mass concentrations of PM_1 and $PM_{2.5}$ are shown in Fig. 3b. The variability in PM_1 and $PM_{2.5}$ mass concentrations was strongly coupled with that in *W*. Others have also found the same

Atmos. Chem. Phys. Discuss., https://doi.org/10.5194/acp-2018-753
Manuscript under review for journal Atmos. Chem. Phys.
Discussion started: 30 July 2018

relationship between W and the mass concentration of $PM_{2.5}$ (e.g., Y.-F. Wang et al., 2012, 2017; Su et al., 2017). Su et al. (2017) suggested that this was due to the aerosol hygroscopic growth effect. To see if this is the true and since aerosol hygroscopicity is highly dependent on the aerosol chemical composition over the North China Plain (Zou et al., 2018), the mass fractions of chemical species of PM_1 are shown in Fig. 3c. As W in the lower atmospheric layer and the mass concentrations of PM_1 and $PM_{2.5}$ increased, the proportion of organic aerosols decreased, suggesting that the proportion of hygroscopic aerosols increased.

Two instances when this relationship was not seen are shown by the black triangles in Fig. 3c. In the evening of 21 May 2016 (the leftmost triangle), the water vapor content was relatively higher. However, the mass concentrations of PM_1 and $PM_{2.5}$ were significantly less than those in the morning of 21 May and the evening of 23 May (the rightmost triangle in Fig. 3c). The mass fractions of organics at the times indicated by the triangles were similar. Su et al. (2017) and Y.-F. Wang et al. (2012, 2017) have studied the relationship between atmospheric water vapor and haze events over Beijing and Xi'an, respectively, using Raman lidar measurements. Their analyses showed a positive correlation between W, and PM_{10} and $PM_{2.5}$ mass concentrations, but they did not analyze in detail the reasons behind some unexpected cases that cropped up. To fully understand this phenomenon, the two cases occurred on 21 May 2016 (Case I) and 23 May 2016 (Case II), were selected for a further study.

4.2 Cases studies of aerosol hygroscopic growth

4.2.1 Lidar-estimated hygroscopic measurements

Cases I and II measurements closest to the radiosonde launch time at 1915 BJT, were first

Atmos. Chem. Phys. Discuss., https://doi.org/10.5194/acp-2018-753
Manuscript under review for journal Atmos. Chem. Phys.
Discussion started: 30 July 2018

selected. Figure 4 shows the vertical distributions of W, θ, the backscattering coefficient at 532 nm (β_{532}), the backscatter-related Ångström exponent (AE) based on measurements at 532 and 1064 nm, and the particle linear depolarization ratio at 532 nm for Case I and Case II. The altitude ranges for each case are 1642.5–1905.5 m for Case I and 1680.0–2130.0 m for Case II. The atmospheric mixing conditions in each layer were examined using W and θ which were calculated from radiosonde-measured temperature and RH profiles. The gradients (in km^{-1}) of the variables within each layer are shown in Table 2. The gradient in W changes little within the layer of interest, decreasing monotonically with altitude at a rate of -0.34 g kg^{-1} km^{-1} and -1.42 g kg^{-1} km^{-1} for Case I and Case II, respectively. The gradient in θ shows a monotonically increase within the layers of interest (0.27°C km^{-1} for Case I and 0.96°C km^{-1} for Case II). Overall, W and θ variations are less than 2 g kg^{-1} and 2°C, respectively, showing that good mixing atmospheric conditions were present in both cases (Granados-Muñoz et al., 2015).

Figure 5 shows the time series of the horizontal wind velocity and direction retrieved from the collocated Doppler lidar system. For Case I within its region of interest (1642.5–1905.0 m), the time series of horizontal wind velocity and direction (Fig. 5a and 5c) at five-minute intervals show that from 1830–2030 BJT, winds over the study area mainly came from the north and had relatively low speeds (< 5 m s^{-1}). Figure 5b and 5d (Case II) show that winds mainly come from the northwest and also had relatively low speeds (< 5 m s^{-1}) within the analyzed layer (1680.0–2130.0 m) from 1830–2030 BJT. This suggests that aerosol particles were transported to Xingtai from the same source region (Bedoya-Velásquez et al., 2018).

The aerosol backscattering coefficients and RH simultaneously increase with altitude in the Case I and Case II layers of interest. The AE and depolarization ratio were retrieved in

Atmos. Chem. Phys. Discuss., https://doi.org/10.5194/acp-2018-753
Manuscript under review for journal Atmos. Chem. Phys.
Discussion started: 30 July 2018

Atmospheric Chemistry and Physics Discussions

order to differentiate the fine/coarse mode predominance and shape of the aerosol particles (Fig. 4e, f, k, and l). A decrease in AE and the depolarization ratio means that there is an increase in the predominance of coarse-mode particles and an increase in the sphericity of particles due to water uptake, respectively (Granados-Muñoz et al., 2015; Lv et al,. 2017; Bedoya-Velásquez et al., 2018).

Based on the aerosol backscattering coefficient at 532 nm and RH profiles retrieved from Raman lidar measurements, the enhancement factor for the backscattering coefficient at 532 nm, $f_\beta(RH)$, is calculated for both cases using Eq. (6). The reference RH value was set to 80% in this study, which is the lowest RH recorded in the layers of interest of both cases. This study applies the two-parameter Kasten model [Eq. (7)] and the one-parameter Hänel model [Eq. (8)]. Table 3 lists the parameterized results of each model for each case and Figure 6 shows the best-fit lines. The enhancement factor for Case II is greater than that for Case I. Specifically, the aerosol backscattering at 532 nm increased by a factor of 1.094 (Case I) and 1.794 (Case II) as RH changed from 80% to 91%. The magnitudes of $f(85\%)$ for Case I and Case II are 1.0283 and 1.0770, respectively. The b value from the Kasten parameterization is much larger in Case II (0.9346) than in Case I (0.1000), and the γ value from Hänel parameterization for Case II (0.6538) is also much greater than that for Case I (0.09895). Chen et al. (2014) studied the aerosol hygroscopicity parameter derived from light-scattering enhancement factor measurements made in the North China Plain and showed that $f(RH)$ for polluted cases is distinctly higher than that for clean periods at a specific RH. This is consistent with the results of this study where the mass concentrations of PM_1 and $PM_{2.5}$ during Case II (69.36 μg m^{-3} for PM_1 and 94.88 μg m^{-3} for $PM_{2.5}$) were greater than those during Case I (34.08 μg m^{-3} for PM_1

and 45.00 μg m^{-3} for $PM_{2.5}$). An observational study of the influence of aerosol hygroscopic growth on the scattering coefficient at a rural area near Beijing also demonstrated that during urban pollution periods, aerosols displayed relatively strong water-absorbing properties (Pan et al., 2009).

4.2.2 The influences of chemical composition inferred from ACSM measurements

Inorganic salt aerosols are mostly hygroscopic by nature, and sulfates and nitrates frequently make up a large part of inorganic aerosols (Tang, 1980). Especially for fine aerosol particles (sizes between 0.1 and 1.0 μm) that scatter visible light more efficiently, the roles of inorganic salt aerosols are often important (Tang, 1996). Liu et al. (2014) have also pointed out that inorganics are the primary aerosol component contributing to aerosol hygroscopicity especially in the size range of 150–1000 nm. The acidity of aerosol particles is a key parameter affecting aerosol hygroscopic growth (Sun et al., 2009; Lv et al., 2017). Generally speaking, neutral aerosols are less hygroscopic than their acidic forms (Zhang et al., 2007). The dominant form of the inorganics can be examined by comparing measured NH_4^+ and predicted NH_4^+ (Lv et al., 2017; see section 3.3 for details).

Figure 7 shows the relationship between measured NH_4^+ and predicted NH_4^+ based on PM_1 chemical species information obtained from the ACSM. The slopes of the linear regression best-fit lines are 0.72 and 0.68 on 21 May 2016 (Case I) and 23 May 2016 (Case II), respectively. The parameter *AV* for Case I is 1.35 and for Case II is 1.50. These values suggest that there was insufficient NH_3 in the atmosphere to neutralize H_2SO_4, HNO_3, and HCl in each case and that the dominant form of inorganics was NH_4NO_3, NH_4HSO_4, and $(NH_4)_2SO_4$. The acidity of

Atmos. Chem. Phys. Discuss., https://doi.org/10.5194/acp-2018-753
Manuscript under review for journal Atmos. Chem. Phys.
Discussion started: 30 July 2018

aerosol particles in Case II is greater than that in Case I, consistent with the results presented here.

A hygroscopicity parameter, kappa (κ), was developed by Petters and Kreidenweis (2007) using chemical composition information (Gysel et al., 2007; Liu et al., 2016; see section 3.4). To further confirm the effect of aerosol hygroscopic growth on haze events, κ is computed for each case based on the dominant form of the inorganics determined previously.

The chemical species obtained from ground-based ACSM measurements of PM_1 around the times of the cases are shown in Fig. 8. In Case I (Fig. 8a), PM_1 was mainly made up of organic particles (39%) and sulfate (39%), followed by nitrate (8%), ammonium (13%), and chloride (1%). In Case II (Fig. 8b), PM_1 was made up of 37% organics, 25% sulfate, 22% nitrate, 12% ammonium, and 1% chloride. Based on the aerosol chemical ion-pairing scheme introduced in Section 3.4 and the aerosol properties shown in Table 1, chloride and organics were neglected because of their relatively small content and comparatively low hygroscopicity (Gysel et al., 2007; Petters and Kreidenweis, 2013). The mass concentrations and volume fractions of NH_4NO_3, NH_4HSO_4, and $(NH_4)_2SO_4$ for each case are given in Table 4. The mass concentration of H_2SO_4 is equal to zero. Liu et al. (2014) have shown that κ for NH_4NO_3, NH_4HSO_4, and $(NH_4)_2SO_4$ is equal to 0.68, 0.56, and 0.60, respectively. Values of κ computed using Eq. (12) are given in Table 4. The parameter κ for Case I (0.557) was less than that for Case II (0.610). This is consistent with our previous results, namely, that the enhancement factor of the backscattering coefficient at 532 nm [$f_\beta(RH)$] for Case II was higher than that for Case I. This suggests that under the same water vapor conditions, the nitrate ion content in aerosol particles can cause significant differences in the hygroscopicity of

aerosols.

4.2.3 Comparison with H-TDMA measurements

Concerning the aerosol scattering enhancement factor, during the last decade, many studies have compared remotely sensed and in situ measurements (using a humidified tandem nephelometer) and shown a positive result (Zieger et al., 2011, 2012; Sheridan et al., 2012; Tesche et al., 2014; Lv et al., 2017). The H-TDMA is also a reliable instrument for use in measuring the aerosol diameter GF due to water uptake (Liu et al., 1978). The aerosol particle diameter GFs observed by the ground-based H-TDMA at the closest time of each case are examined next.

Table 5 lists H-TDMA-derived aerosol particle size hygroscopic GFs at an RH level of ~85% for different particle sizes. All aerosol particle size hygroscopic GFs for Case II are higher than those for Case I. GFs for different aerosol particle sizes in both cases were extrapolated to different RH levels using Eq. (3) from Gysel et al. (2009) who used the kappa model introduced by Petters and Kreidenwies (2007). Figure 9 shows that Case II aerosol particle size hygroscopic GFs at each RH level (80–91%) are higher than those of Case I. Although the aerosol backscattering enhancement factor and aerosol particle GF are completely different parameters for calculating the hygroscopicity of aerosol particles and are difficult to compare quantitatively, the H-TDMA results offer a sense of confidence that aerosol hygroscopicity has an important influence on the formation of heavy haze.

In general, both the lidar-estimated aerosol hygroscopic enhancement factor and the ACSM and H-TDMA measurements support the proposed hypothesis that the main reason for

Atmos. Chem. Phys. Discuss., https://doi.org/10.5194/acp-2018-753
Manuscript under review for journal Atmos. Chem. Phys.
Discussion started: 30 July 2018

the variability in PM_1 and $PM_{2.5}$ mass concentrations is strongly coupled with that in W which has to do with the different hygroscopic properties of aerosols.

5. Conclusions

During late May 2016, the W over Xingtai was generally less than 6 g kg^{-1} with a strong daily variability. Overall, the simultaneous temporal change of the mass concentrations of PM_1 and $PM_{2.5}$ was strongly associated with that of atmospheric water vapor content due to the hygroscopicity of the aerosol particles. Two cases where this relationship was not seen were identified and further examined. Case I represents a relatively clean case and Case II represents a polluted case. The γ value from the Hänel parameterization for Case II (0.6538) was larger than that for Case I (0.09895). A key parameter affecting the hygroscopicity of aerosol particles, namely, acid value, was examined by comparing measured NH_4^+ and predicted NH_4^+. The acid value for Case I (1.35) was less than that for Case II (1.50) and the main form of inorganics was NH_4NO_3, NH_4HSO_4, and $(NH_4)_2SO_4$. The aerosol chemical composition determined by the ACSM showed that the value of the aerosol hygroscopicity parameter κ for Case II (0.610) was greater than that for Case I (0.577) due to the greater mass fraction of nitrate salt. H-TDMA measurements showed that the hygroscopic GF in each particle size category (40, 80, 110, 150, and 200 nm) for Case II was greater than that for Case I.

The aerosol backscattering enhancement factor [$f_\beta(RH)$], the aerosol particle growth factor, the aerosol acidity, and the hygroscopicity parameter are completely different quantities for calculating the hygroscopicity of aerosol particles and are difficult to compare quantitatively. The lidar-estimated aerosol hygroscopic enhancement factor and ACSM and H-TDMA

measurements show that the hygroscopic growth of aerosol particles has a strong influence on the process of air pollution. Under the same atmospheric water vapor content conditions, the stronger the hygroscopicity of aerosols, the more likely they cause severe air pollution. The mass fraction of the nitrate ion in aerosol particles was one of the main factors that determined the hygroscopic ability of aerosols in the study area (Xingtai). These findings not only reveal a major cause of air pollution but also provide a scientific basis for the local government to put more effort into preventing and controlling environmental contamination in this commonly known as the most polluted place in China.

Add acknowledgements

This work was supported by the National Key R&D Program of China (2017YFC1501702), the National Science Foundation of China (91544217), and the US National Science Foundation (AGS1534670).

Atmos. Chem. Phys. Discuss., https://doi.org/10.5194/acp-2018-753
Manuscript under review for journal Atmos. Chem. Phys.
Discussion started: 30 July 2018

Atmospheric Chemistry and Physics Discussions

References

Barnes, J. E., Kaplan, T., Vömel, H. and Read, W. G.: NASA/Aura/Microwave Limb Sounder water vapor validation at Mauna Loa Observatory by Raman lidar, J. Geophys. Res., 113(D15), D15S03, doi:10.1029/2007JD008842, 2008.

Bedoya-Velásquez, A. E., Navas-Guzmán, F., Granados-Muñoz, M. J., Titos, G., Román, R., Andrés Casquero-Vera, J., Ortiz-Amezcua, P., Antonio Benavent-Oltra, J., De Arruda Moreira, G., Montilla-Rosero, E., Hoyos, C. D., Artiñano, B., Coz, E., Olmo-Reyes, F. J., Alados-Arboledas, L. and Guerrero-Rascado, J. L.: Hygroscopic growth study in the framework of EARLINET during the SLOPE i campaign: Synergy of remote sensing and in situ instrumentation, Atmos. Chem. Phys., 18(10), 7001–7017, doi:10.5194/acp-18-7001-2018, 2018.

Bucholtz, A.: Rayleigh-scattering calculations for the terrestrial atmosphere, Appl. Opt., 34(15), 2765, doi:10.1364/AO.34.002765, 1995.

Carrico, C. M., Petters, M. D., Kreidenweis, S. M., Sullivan, A. P., McMeeking, G. R., Levin, E. J. T., Engling, G., Malm, W. C. and Collett, J. L.: Water uptake and chemical composition of fresh aerosols generated in open burning of biomass, Atmos. Chem. Phys., doi:10.5194/acp-10-5165-2010, 2010.

Chen, J., Zhao, C. S., Ma, N. and Yan, P.: Aerosol hygroscopicity parameter derived from the light scattering enhancement factor measurements in the North China Plain, Atmos. Chem. Phys., 14(15), 8105–8118, doi:10.5194/acp-14-8105-2014, 2014.

Covert, D. S., Charlson, R. J. and Ahlquist, N. C.: A Study of the Relationship of

Chemical Composition and Humidity to Light Scattering by Aerosols, J. Appl. Meteorol., 11(6), 968–976, doi:10.1175/1520-0450(1972)011<0968:ASOTRO>2.0.CO;2, 1972.

Di Girolamo, P., Summa, D., Bhawar, R., Di Iorio, T., Cacciani, M., Veselovskii, I., Dubovik, O. and Kolgotin, A.: Raman lidar observations of a Saharan dust outbreak event: Characterization of the dust optical properties and determination of particle size and microphysical parameters, Atmos. Environ., doi:10.1016/j.atmosenv.2011.12.061, 2012.

Fernald, F. G.: Analysis of atmospheric lidar observations: some comments, Appl. Opt., doi:10.1364/AO.23.000652, 1984.

Feingold, G. and Morley, B.: Aerosol hygroscopic properties as measured by lidar and comparison with in situ measurements, J. Geophys. Res., 108(D11), 4327, doi:10.1029/2002JD002842, 2003.

Fernández, A. J., Apituley, A., Veselovskii, I., Suvorina, A., Henzing, J., Pujadas, M. and Artíñano, B.: Study of aerosol hygroscopic events over the Cabauw experimental site for atmospheric research (CESAR) using the multi-wavelength Raman lidar Caeli, Atmos. Environ., 120, 484–498, doi:10.1016/j.atmosenv.2015.08.079, 2015.

Fountoukis, C. and Nenes, A.: ISORROPIA II: a computationally efficient thermodynamic equilibrium model for K+–Ca2+–Mg2+–NH4+–Na+–SO42−–NO3, Atmos. Chem. Phys., 7(17), 4639–4659, doi:10.5194/acp-7-4639-2007, 2007.

Froidevaux, M., Higgins, C. W., Simeonov, V., Ristori, P., Pardyjak, E., Serikov, I.,

Calhoun, R., Bergh, H. van den and Parlange, M. B.: A Raman lidar to measure water vapor in the atmospheric boundary layer, Adv. Water Resour., doi:10.1016/j.advwatres.2012.04.008, 2013.

Granados-Muñoz, M. J., Navas-Guzmán, F., Bravo-Aranda, J. A., Guerrero-Rascado, J. L., Lyamani, H., Valenzuela, A., Titos, G., Fernández-Gálvez, J. and Alados-Arboledas, L.: Hygroscopic growth of atmospheric aerosol particles based on active remote sensing and radiosounding measurements: Selected cases in southeastern Spain, Atmos. Meas. Tech., doi:10.5194/amt-8-705-2015, 2015.

Gysel, M., Crosier, J., Topping, D. O., Whitehead, J. D., Bower, K. N., Cubison, M. J., Williams, P. I., Flynn, M. J., McFiggans, G. B. and Coe, H.: Closure study between chemical composition and hygroscopic growth of aerosol particles during TORCH2, Atmos. Chem. Phys., doi:10.5194/acp-7-6131-2007, 2007.

Gysel, M., McFiggans, G. B. and Coe, H.: Inversion of tandem differential mobility analyser (TDMA) measurements, J. Aerosol Sci., doi:10.1016/j.jaerosci.2008.07.013, 2009.

Hänel, G.: The properties of atmospheric aerosol particles as functions of the relative humidity at thermodynamic equilibrium with the surrounding moist air, Adv. Geophys., doi:10.1016/S0065-2687(08)60142-9, 1976.

Haywood, J., Bush, M., Abel, S., Claxton, B., Coe, H., Crosier, J., Harrison, M., Macpherson, B., Naylor, M. and Osborne, S.: Prediction of visibility and aerosol within the operational Met Office Unified Model. II: Validation of model

performance using observational data, Q. J. R. Meteorol. Soc., doi:10.1002/qj.275, 2008.

Jeong, M. J., Li, Z., Andrews, E. and Tsay, S. C.: Effect of aerosol humidification on the column aerosol optical thickness over the Atmospheric Radiation Measurement Southern Great Plains site, J. Geophys. Res. Atmos., doi:10.1029/2006JD007176, 2007.

Kasten, F.: Visibility forecast in the phase of pre-condensation, Tellus, doi:10.3402/tellusa.v21i5.10112, 1969.

Kotchenruther, R. A., Hobbs, P. V. and Hegg, D. A.: Humidification factors for atmospheric aerosols off the mid-Atlantic coast of the United States, J. Geophys. Res. Atmos., doi:10.1029/98JD01751, 1999.

Leblanc, T., McDermid, I. S. and Walsh, T. D.: Ground-based water vapor raman lidar measurements up to the upper troposphere and lower stratosphere for long-term monitoring, Atmos. Meas. Tech., doi:10.5194/amt-5-17-2012, 2012.

Liu, B. Y. H., Pui, D. Y. H., Whitby, K. T., Kittelson, D. B., Kousaka, Y. and McKenzie, R. L.: The aerosol mobility chromatograph: A new detector for sulfuric acid aerosols, Atmos. Environ., doi:10.1016/0004-6981(78)90192-0, 1978.

Liu, H. J., Zhao, C. S., Nekat, B., Ma, N., Wiedensohler, A., Van Pinxteren, D., Spindler, G., Müller, K. and Herrmann, H.: Aerosol hygroscopicity derived from size-segregated chemical composition and its parameterization in the North China Plain, Atmos. Chem. Phys., doi:10.5194/acp-14-2525-2014, 2014.

Liu, Y. C., Wu, Z. J., Tan, T. Y., Wang, Y. J., Qin, Y. H., Zheng, J., Li, M. R. and Hu, M.: Estimation of the PM2.5 effective hygroscopic parameter and water content based on particle chemical composition: Methodology and case study, Sci. China Earth Sci., doi:10.1007/s11430-016-5313-9, 2016.

Lv, M., Liu, D., Li, Z., Mao, J., Sun, Y., Wang, Z., Wang, Y. and Xie, C.: Hygroscopic growth of atmospheric aerosol particles based on lidar, radiosonde, and in situ measurements: Case studies from the Xinzhou field campaign, J. Quant. Spectrosc. Radiat. Transf., 188, 60–70, doi:10.1016/j.jqsrt.2015.12.029, 2017.

MacKinnon, D. J.: The Effect of Hygroscopic Particles on the Backscattered Power from a Laser Beam, Atmos. Sci., 26, 500-510, 1969.

Melfi, S. H.: Remote measurements of the atmosphere using {Raman} scattering, Appl. Opt., doi:10.1364/AO.11.001605, 1972.

Mie G.: Beiträge zur Optik trüber Medien, speziell kolloidaler Metallösungen, Ann. Phys., 25, 377-455, 1908.

Pahlow, M., Feingold, G., Jefferson, A., Andrews, E., Ogren, J. A., Wang, J., Lee, Y. N., Ferrare, R. A. and Turner, D. D.: Comparison between lidar and nephelometer measurements of aerosol hygroscopicity at the Southern Great Plains Atmospheric Radiation Measurement site, J. Geophys. Res. Atmos., doi:10.1029/2004JD005646, 2006.

Pan, X. L., Yan, P., Tang, J., Ma, J. Z., Wang, Z. F., Gbaguidi, A. and Sun, Y. L.: Observational study of influence of aerosol hygroscopic growth on scattering

coefficient over rural area near Beijing mega-city, Atmos. Chem. Phys., doi:10.5194/acp-9-7519-2009, 2009.

Petters, M. D. and Kreidenweis, S. M.: A single parameter representation of hygroscopic growth and cloud condensation nucleus activity, Atmos. Chem. Phys., 7, 1961-1971, doi:10.5194/acp-7-1961-2007, 2007.

Petters, M. D. and Kreidenweis, S. M.: A single parameter representation of hygroscopic growth and cloud condensation nucleus activity-Part 3: Including surfactant partitioning, Atmos. Chem. Phys., doi:10.5194/acp-13-1081-2013, 2013.

Reilly, P. J. and Wood, R. H.: The prediction of the properties of mixed electrolytes from measurements on common ion mixtures, J. Phys. Chem., doi:10.1021/j100846a043, 1969.

Sheridan, P. J., Andrews, E., Ogren, J. A., Tackett, J. L. and Winker, D. M.: Vertical profiles of aerosol optical properties over central Illinois and comparison with surface and satellite measurements, Atmos. Chem. Phys., doi:10.5194/acp-12-11695-2012, 2012.

Sherlock, V., Hauchecorne, A., and Lenoble, J.: Methodology for the independent calibration of Raman backscatter water-vapor lidar systems, Appl. Opt., doi:10.1364/AO.38.005816, 1999.

Stokes, R. H. and Robinson, R. A.: Interactions in aqueous nonelectrolyte solutions. I. Solute-solvent equilibria, J. Phys. Chem., doi:10.1021/j100879a010, 1966.

Su, T., Li, J., Li, J., Li, C., Chu, Y., Zhao, Y., Guo, J., Yu, Y. and Wang, L.: The Evolution of Springtime Water Vapor over Beijing Observed by a High Dynamic Raman Lidar System: Case Studies, IEEE J. Sel. Top. Appl. Earth Obs. Remote Sens., doi:10.1109/JSTARS.2017.2653811, 2017.

Sun, J., Zhang, Q., Canagaratna, M. R., Zhang, Y., Ng, N. L., Sun, Y., Jayne, J. T., Zhang, X., Zhang, X. and Worsnop, D. R.: Highly time- and size-resolved characterization of submicron aerosol particles in Beijing using an Aerodyne Aerosol Mass Spectrometer, Atmos. Environ., doi:10.1016/j.atmosenv.2009.03.020, 2009.

Sun, Y., Chen, C., Zhang, Y., Xu, W., Zhou, L., Cheng, X., Zheng, H., Ji, D., Li, J., Tang, X., Fu, P. and Wang, Z.: Rapid formation and evolution of an extreme haze episode in Northern China during winter 2015, Sci. Rep., doi:10.1038/srep27151, 2016.

Swietlicki, E., Hansson, H. C., Hämeri, K., Svenningsson, B., Massling, A., Mcfiggans, G., Mcmurry, P. H., Petäjä, T., Tunved, P., Gysel, M., Topping, D., Weingartner, E., Baltensperger, U., Rissler, J., Wiedensohler, A. and Kulmala, M.: Hygroscopic properties of submicrometer atmospheric aerosol particles measured with H-TDMA instruments in various environments - A review, Tellus, Ser. B Chem. Phys. Meteorol., doi:10.1111/j.1600-0889.2008.00350.x, 2008.

Tang, I. N.: Deliquescence properties and particle size change of hygroscopic aerosols, AGARD Rep., 153-167, 1980.

Tang, I. N.: Chemical and size effects of hygroscopic aerosols on light scattering

coefficients, J. Geophys. Res. Atmos., 101(D14), 19245–19250, doi:10.1029/96JD03003, 1996.

Tang, I. N. and Munkelwitz, H. R.: Water activities, densities, and refractive indices of aqueous sulfates and sodium nitrate droplets of atmospheric importance, J. Geophys. Res., doi:10.1029/94JD01345, 1994.

Tardif, R.: Boundary Layer a Erosol Backscattering and Its Relationship To Relative Humidity From a Combined Raman – Elastic backscatter lidar, Class Project for ATOC 5235 Remote Sensing of the Atmosphere and Oceanic. University of Colorado, 2002.

Tesche, M., Zieger, P., Rastak, N., Charlson, R. J., Glantz, P., Tunved, P. and Hansson, H. C.: Reconciling aerosol light extinction measurements from spaceborne lidar observations and in situ measurements in the Arctic, Atmos. Chem. Phys., doi:10.5194/acp-14-7869-2014, 2014.

Tie, X., Huang, R. J., Cao, J., Zhang, Q., Cheng, Y., Su, H., Chang, D., Pöschl, U., Hoffmann, T., Dusek, U., Li, G., Worsnop, D. R. and O'Dowd, C. D.: Severe Pollution in China Amplified by Atmospheric Moisture, Sci. Rep., doi:10.1038/s41598-017-15909-1, 2017.

Titos, G., Cazorla, A., Zieger, P., Andrews, E., Lyamani, H., Granados-Muñoz, M. J., Olmo, F. J. and Alados-Arboledas, L.: Erratum to 'Effect of hygroscopic growth on the aerosol light-scattering coefficient: A review of measurements, techniques and error sources' [Atmos. Environ. 141C (2016) 494–507] (S1352231016305404)

(10.1016/j.atmosenv.2016.07.021)), Atmos. Environ., doi:10.1016/j.atmosenv.2018.02.030, 2018.

Tobin, I., Bony, S. and Roca, R.: Observational evidence for relationships between the degree of aggregation of deep convection, water vapor, surface fluxes, and radiation, J. Clim., doi:10.1175/JCLI-D-11-00258.1, 2012.

Twomey, S.: The Influence of Pollution on the Shortwave Albedo of Clouds, J. Atmos. Sci., doi:10.1175/1520-0469(1977)034<1149:TIOPOT>2.0.CO;2, 1977.

Veselovskii, I., Whiteman, D. N., Kolgotin, A., Andrews, E. and Korenskii, M.: Demonstration of aerosol property profiling by multiwavelength lidar under varying relative humidity conditions, J. Atmos. Ocean. Technol., doi:10.1175/2009JTECHA1254.1, 2009.

Wang, W., Gong, W., Mao, F. and Zhang, J.: Long-term measurement for low-tropospheric water vapor and aerosol by Raman Lidar in Wuhan, Atmosphere (Basel)., 6(4), 521–533, doi:10.3390/atmos6040521, 2015.

Wang, Y.-F., Hua, D., Wang, L., Tang, J., Mao, J. and Kobayashi, T.: Observations and analysis of relationship between water vapor and aerosols by using raman lidar, Jpn. J. Appl. Phys., doi:10.1143/JJAP.51.102401, 2012.

Wang, Y. -F., Zhang, J., Fu, Q., Song, Y., Di, H., Li, B. and Hua, D.: Variations in the water vapor distribution and the associated effects on fog and haze events over Xi'an based on Raman lidar data and back trajectories, Appl. Opt., doi:10.1364/AO.56.007927, 2017.

Wang, Y.-Y., Zhang, F., Li, Z., Tan, H., Xu, H., Ren, J., Zhao, J., Du, W. and Sun, Y.: Enhanced hydrophobicity and volatility of submicron aerosols under severe emission control conditions in Beijing, Atmos. Chem. Phys., doi:10.5194/acp-17-5239-2017, 2017.

Whiteman, D. N.: Examination of the traditional Raman lidar technique II Evaluating the ratios for water vapor and aerosols, Appl. Opt., doi:10.1364/AO.42.002593, 2003.

Yan, X., Shi, W., Li, Z., Li, Z., Luo, N., Zhao, W., Wang, H. and Yu, X.: Satellite-based PM2.5estimation using fine-mode aerosol optical thickness over China, Atmos. Environ., doi:10.1016/j.atmosenv.2017.09.023, 2017.

Zdanovskii, A. B.: New methods for calculating solubilities of electrolytes in multi-component systems, Zhur. Fiz. Khim., 22, 1475-1485, 1948.

Zhang, L., Sun, J. Y., Shen, X. J., Zhang, Y. M., Che, H., Ma, Q. L., Zhang, Y. W., Zhang, X. Y. and Ogren, J. A.: Observations of relative humidity effects on aerosol light scattering in the Yangtze River Delta of China, Atmos. Chem. Phys., doi:10.5194/acp-15-8439-2015, 2015.

Zhang, Q., Jimenez, J. L., Worsnop, D. R. and Canagaratna, M.: A case study of urban particle acidity and its influence on secondary organic aerosol., Environ. Sci. Technol., doi:10.1021/es061812j, 2007.

Zhang, Y., Sun, Y., Du, W., Wang, Q., Chen, C., Han, T., Lin, J., Zhao, J., Xu, W., Gao, J., Li, J., Fu, P., Wang, Z. and Han, Y.: Response of aerosol composition to different emission scenarios in Beijing, China, Sci. Total Environ.,

doi:10.1016/j.scitotenv.2016.07.073, 2016.

Zhang, Y., Du, W., Wang, Y., Wang, Q., Wang, H., Zheng, H., Zhang, F., Shi, H., Bian, Y., Han, Y., Fu, P., Canonaco, F., Prévôt, A. S. H., Zhu, T., Wang, P., Li, Z. and Sun, Y.: Aerosol chemistry and particle growth events at an urban downwind site in North China Plain, Atmos. Chem. Phys. Discuss., doi:10.5194/acp-2017-889, 2017.

Zieger, P., Weingartner, E., Henzing, J., Moerman, M., De Leeuw, G., Mikkilä, J., Ehn, M., Petäjä, T., Clémer, K., Van Roozendael, M., Yilmaz, S., Frieß, U., Irie, H., Wagner, T., Shaiganfar, R., Beirle, S., Apituley, A., Wilson, K. and Baltensperger, U.: Comparison of ambient aerosol extinction coefficients obtained from in-situ, MAX-DOAS and LIDAR measurements at Cabauw, Atmos. Chem. Phys., doi:10.5194/acp-11-2603-2011, 2011.

Zieger, P., Kienast-Sjögren, E., Starace, M., Von Bismarck, J., Bukowiecki, N., Baltensperger, U., Wienhold, F. G., Peter, T., Ruhtz, T., Collaud Coen, M., Vuilleumier, L., Maier, O., Emili, E., Popp, C. and Weingartner, E.: Spatial variation of aerosol optical properties around the high-alpine site Jungfraujoch (3580 m a.s.l.), Atmos. Chem. Phys., doi:10.5194/acp-12-7231-2012, 2012.

Zieger, P., Fierz-Schmidhauser, R., Poulain, L., Müller, T., Birmili, W., Spindler, G., Wiedensohler, A., Baltensperger, U. and Weingartner, E.: Influence of water uptake on the aerosol particle light scattering coefficients of the Central European aerosol, Tellus, Ser. B Chem. Phys. Meteorol., doi:10.3402/tellusb.v66.22716, 2014.

Zou, J., Liu, Z., Hu, B., Huang, X., Wen, T., Ji, D., Liu, J., Yang, Y., Yao, Q. and Wang,

Y.: Aerosol chemical compositions in the North China Plain and the impact on the visibility in Beijing and Tianjin, Atmos. Res., doi:10.1016/j.atmosres.2017.09.014, 2018.

Atmos. Chem. Phys. Discuss., https://doi.org/10.5194/acp-2018-753
Manuscript under review for journal Atmos. Chem. Phys.
Discussion started: 30 July 2018

Atmospheric Chemistry and Physics Discussions

Table 1. Aerosol properties of selected compounds used for the calculation of the hygroscopicity parameter κ, i.e., the density (ρ_i) and (κ_i) of each compound.

species	NH_4NO_3	NH_4HSO_4	$(NH_4)_2SO_4$	H_2SO_4
density[a]	1.725	1.78	1.76	1.83
κ [b]	0.68	0.56	0.52	0.91

(a) Tang and Munkelwitz (1994); Carrico et al. (2010);

(b) Fountoukis and Nenes (2007); Carrico et al. (2010); Liu et al. (2014).

Atmos. Chem. Phys. Discuss., https://doi.org/10.5194/acp-2018-753
Manuscript under review for journal Atmos. Chem. Phys.
Discussion started: 30 July 2018

Atmospheric Chemistry and Physics Discussions

Table 2. Range of values and gradient values over the analyzed layer for the water vapor mixing ratio (*W*), the potential temperature (θ), the backscattering coefficient at 532 nm (β_{532}), the Ångström exponent [AE (532–1064 nm)], and the depolarization ratio at 532 nm for Cases I and II.

	Case I			Case Ⅱ		
	Range		Gradient (km^{-1})	Range		Gradient (km^{-1})
Altitude (m)	1642.5	1905.0	—	1680.0	2130.0	—
W ($g\ kg^{-1}$)	7.65	7.56	-0.34	6.42	5.78	-1.42
θ (℃)	26.93	27.00	0.27	25.18	25.61	0.96
RH (%)	80	91	—	80	91	—
β_{532nm} ($km^{-1}\ sr^{-1}$)	0.01379	0.01535	—	0.003711	0.006762	—
AE (532–1064 nm)	0.74	0.68	-0.23	0.42	0.35	-0.16
Depolarization ratio	0.046	0.044	-0.0076	0.041	0.039	-0.0044

Atmos. Chem. Phys. Discuss., https://doi.org/10.5194/acp-2018-753
Manuscript under review for journal Atmos. Chem. Phys.
Discussion started: 30 July 2018

Atmospheric Chemistry and Physics Discussions

Table 3. The fitting parameters and R^2 of the fit for the Kasten and Hänel models.

	Case I			Case II		
	a	b	R^2	a	b	R^2
Kasten model	0.8508	0.1000	0.97	0.1916	0.9346	0.95
	γ		R^2	γ		R^2
Hänel model	0.09895±0.0047		0.97	0.6538±0.0662		0.84

Table 4. Calculated mass concentrations and volume fractions of NH_4NO_3, NH_4HSO_4, and $(NH_4)_2SO_4$, and the hygroscopicity parameter (κ) for Case I and Case II.

	Case I			Case II		
	NH_4NO_3	NH_4HSO_4	$(NH_4)_2SO_4$	NH_4NO_3	NH_4HSO_4	$(NH_4)_2SO_4$
mass conc. ($\mu g\ m^{-3}$)	3.60	8.31	8.30	12.2979	10.3795	3.0616
volume fraction	0.18	0.41	0.41	0.48	0.40	0.12
κ		0.557			0.610	

Atmos. Chem. Phys. Discuss., https://doi.org/10.5194/acp-2018-753
Manuscript under review for journal Atmos. Chem. Phys.
Discussion started: 30 July 2018

Atmospheric Chemistry and Physics Discussions

Table 5. Different aerosol particle size hygroscopic growth factors at a relative humidity level of ~85% for Case I and Case II.

	GF(85%, D_p)				
	40 nm	80 nm	110 nm	150 nm	200 nm
Case I	1.32	1.36	1.39	1.40	1.41
Case II	1.33	1.39	1.40	1.41	1.42

Atmos. Chem. Phys. Discuss., https://doi.org/10.5194/acp-2018-753
Manuscript under review for journal Atmos. Chem. Phys.
Discussion started: 30 July 2018

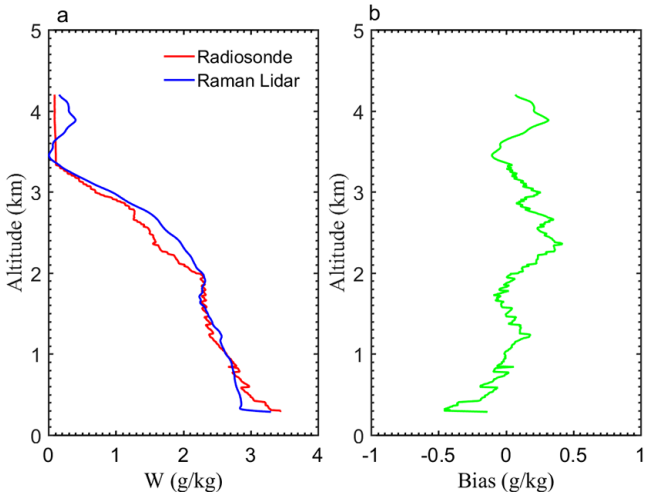

Fig. 1. (a) Water vapor mixing ratios at 0515 BJT 24 May 2016 retrieved by the Raman lidar (blue line) and the radiosonde (red dashed line) and (b) the difference between them (lidar minus radiosonde).

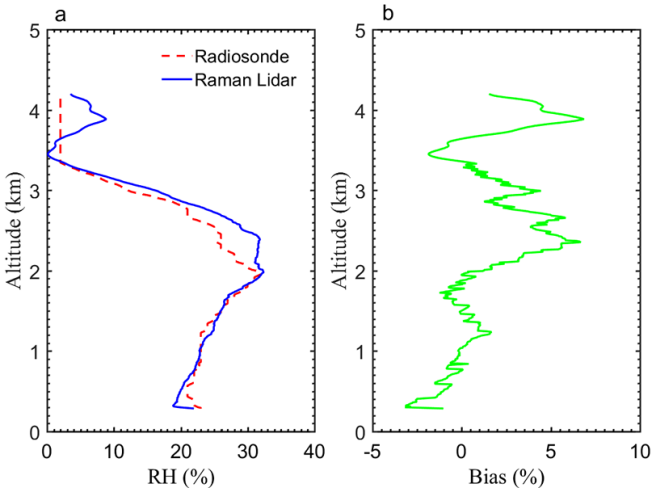

Fig. 2. Relative humidity at 0515 BJT 24 May 2016 retrieved by the Raman lidar (blue line) and the radiosonde (red dashed line) and (b) the difference between them (lidar minus radiosonde).

Atmos. Chem. Phys. Discuss., https://doi.org/10.5194/acp-2018-753
Manuscript under review for journal Atmos. Chem. Phys.
Discussion started: 30 July 2018

Atmospheric Chemistry and Physics Discussions

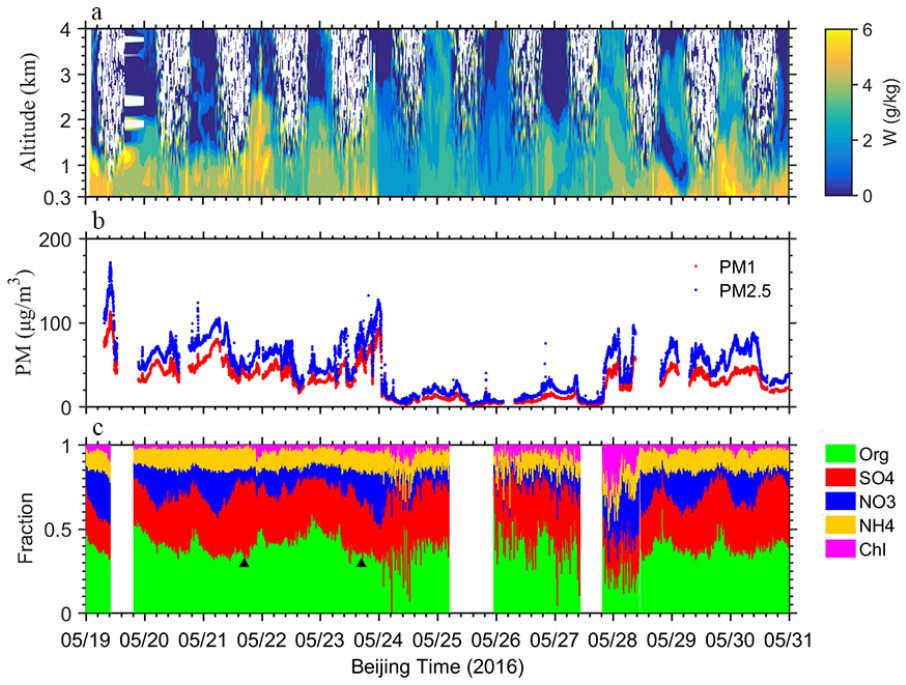

Fig. 3. Time series of (a) water vapor mixing ratio (*W*) profiles measured by the Raman lidar, (b) mass concentrations of PM_1 (red dots) and $PM_{2.5}$ (blue dots), and (c) chemical species mass fractions of PM_1 measured by the ACSM. Data are from 19–31 May 2016 at Xingtai. The black triangles in (c) represent the two cases chosen for further examination.

Atmos. Chem. Phys. Discuss., https://doi.org/10.5194/acp-2018-753
Manuscript under review for journal Atmos. Chem. Phys.
Discussion started: 30 July 2018

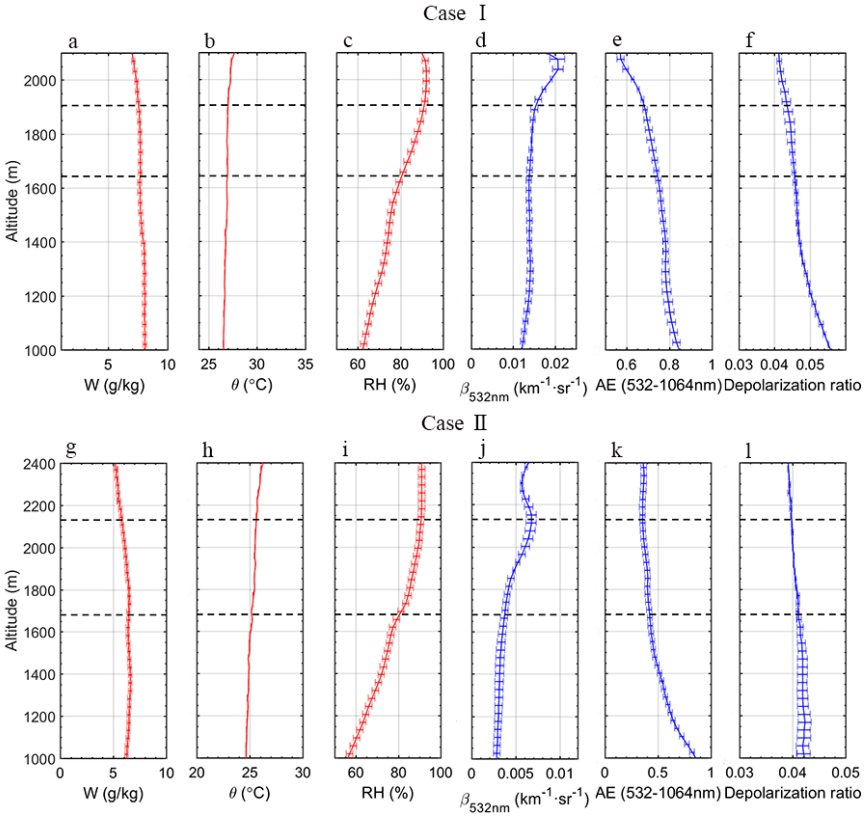

Fig. 4. The vertical profiles of (a, g) water vapor mixing ratio (W), (b, h) potential temperature (θ), (c, i) relative humidity (RH) calculated from radiosonde data, (d, j) backscattering coefficient at 532 nm (β_{532}), (e, k) the Angstrom exponent [AE (532-1064nm)], (f, l) depolarization ratio retrieved from Raman lidar data for Case I (top panels) and Case II (bottom panels). Horizontal dashed lines show the upper and lower boundaries of the layer under analysis (1642.5–1905.0 m for Case I and 1680.0–2130.0 m for Case II).

Atmos. Chem. Phys. Discuss., https://doi.org/10.5194/acp-2018-753
Manuscript under review for journal Atmos. Chem. Phys.
Discussion started: 30 July 2018

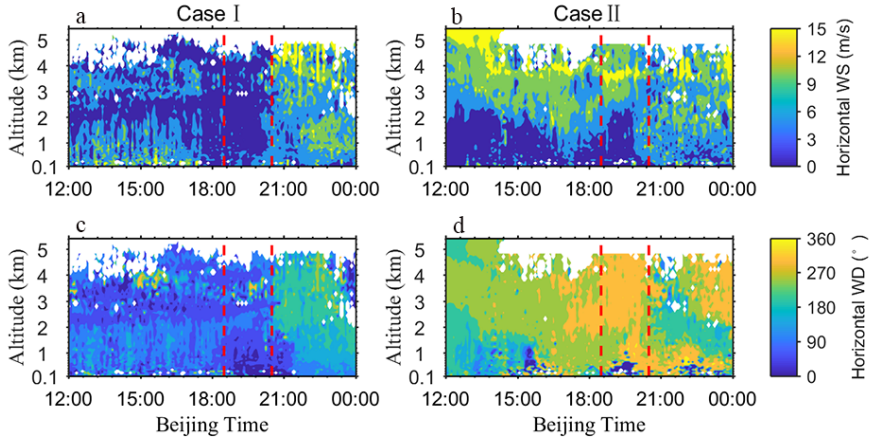

Fig. 5. Time series of Doppler-lidar-retrieved (a, b) horizontal wind speed and (c, d) horizontal wind direction on 21 May 2016 (Case I, left-hand panels) and 23 May 2016 (Case II, right-hand panels). Red dashed lines outline the time range 1830–2030 BJT. The analyzed layers are 1642.5–1905.0 m for Case I and 1680.0–2130.0 m for Case II.

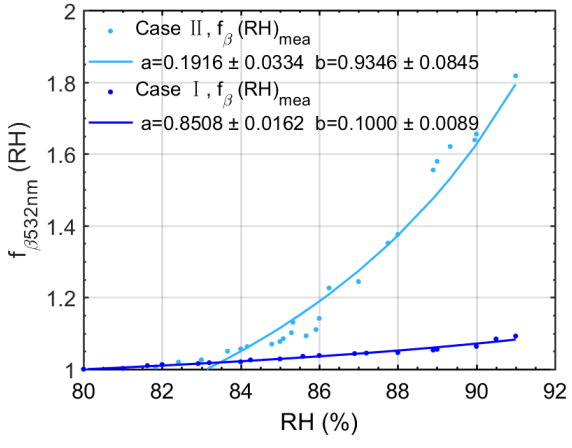

Fig. 6. *f(RH)* at 532 nm retrieved on 21 May 2016 in the 1642.5–1905.0 m layer (Case I, dark blue points) and 23 May 2016 in the 1680.0–2130.0 m layer (Case II, light blue points). The best-fit lines through the points are shown. The reference RH is 80%.

Atmos. Chem. Phys. Discuss., https://doi.org/10.5194/acp-2018-753
Manuscript under review for journal Atmos. Chem. Phys.
Discussion started: 30 July 2018

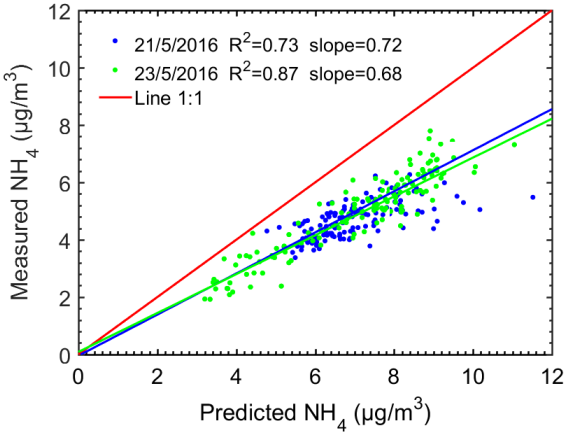

Fig. 7. Mass concentrations of measured ammonium (NH_4) versus predicted ammonium assuming full neutralization of sulfate, nitrate and chloride for Case I (blue dots) on 21 May 2016 and Case II (green dots) on 23 May 2016. The solid blue and green lines are the least-squares regression lines for Case I and Case II, respectively. The 1:1 line is shown in red.

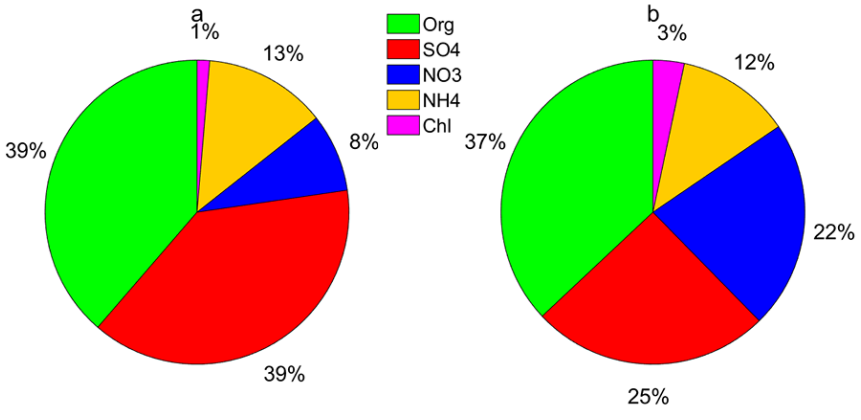

Fig. 8. Aerosol mass fractions of PM_1 measured by the ACSM on (a) 21 May 2016 (Case I) and (b) 23 May 2016 (Case II).

Atmos. Chem. Phys. Discuss., https://doi.org/10.5194/acp-2018-753
Manuscript under review for journal Atmos. Chem. Phys.
Discussion started: 30 July 2018

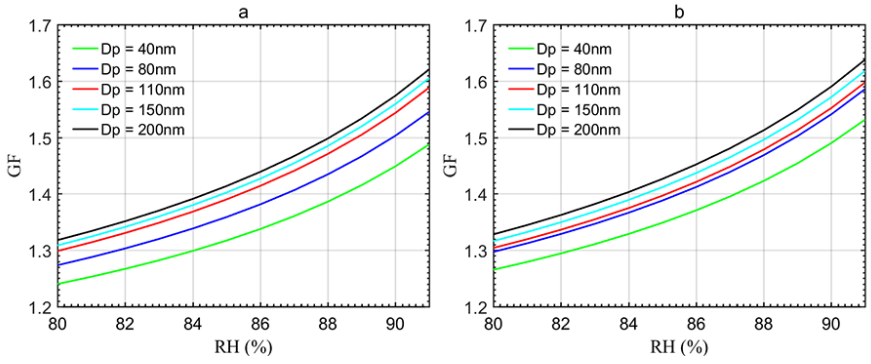

Fig. 9. Aerosol particle size hygroscopic growth factor (GF) as a function of relative humidity (RH) for (a) Case I and (b) Case II. The different colors represent different particle sizes (Dp).